

FLUID FLOW AND INCLUSION REMOVAL IN MOLTEN STEEL CONTINUOUS CASTING STRANDS

Lifeng ZHANG

Professor, Dept. of Materials Science & Engineering, Norwegian University of Science & Technology (NTNU)

Alfred Getz vei 2, N-7491 Trondheim, Norway, Email: lifeng.zhang@material.ntnu.no

<http://www.nt.ntnu.no/users/lifengz/>

ABSTRACT

Turbulent flow, the transport of inclusions and bubbles, and inclusion removal by fluid flow transport and by bubble flotation in the strand of the continuous slab caster are investigated using computational models, and validated through comparison with plant measurements of inclusions. Steady 3-D flow of steel in the liquid pool in the mold and upper strand is simulated with a finite-difference computational model using the standard k- ϵ turbulence model. Trajectories of inclusions and bubbles are calculated by integrating each local velocity, considering its drag and buoyancy forces. A "random walk" model is used to incorporate the effect of turbulent fluctuations on the particle motion. The attachment probability of inclusions on a bubble surface is investigated based on fundamental fluid flow simulations, incorporating the turbulent inclusion trajectory and sliding time of each individual inclusion along the bubble surface as a function of particle and bubble size. The change in inclusion distribution due to removal by bubble transport in the mold is calculated based on the computed attachment probability of inclusion on each bubble and the computed path length of the bubbles. Results indicate that 6-10% inclusions are removed by fluid flow transport, 10% by bubble flotation, and 4% by entrapment to the SEN walls. Smaller bubbles and larger inclusions have larger attachment probabilities. Smaller bubbles are more efficient at inclusion removal by bubble flotation, so long as they are not entrapped in the solidifying shell. Larger gas flow rate favors inclusion removal by bubble flotation. The optimum bubble size should be 2-4mm.

INTRODUCTION

Increasing the productivity and improving the product quality are permanent requirements concerning the continuous casting process. To produce clean steel with as few inclusions as possible is one of the main tasks of steelmakers. Inclusions can be removed from the molten steel by fluid flow transport or by bubble flotation¹⁻⁶. Inclusions attached to the surface of bubbles can be removed faster due to the small residence time of bubbles in the molten steel. However, bubbles with attached inclusions can finally generate line defects such as blisters and pencil pipes if they are entrapped to the solidified shell.^{7,8} **Figure 1** is the example of bubbles with attached inclusions^{9,10}.

Plant observations have found that many serious quality problems, including inclusion entrapment, are directly associated with the flow pattern in the mold.¹¹ Thus

design and control of the fluid flow pattern in the continuous casting mold to remove inclusions is of crucial importance to the steel industry. The flow pattern in the mold can be controlled by many variables, including the nozzle and mold geometry, submergence depth, steel flow rate, argon injection rate, electromagnetic stirring, and flux layer properties. Nozzle technology is an easy and inexpensive way to optimize the fluid flow in the mold. New techniques involving the Submergence Entry Nozzle (SEN) to improve the fluid flow pattern and inclusion removal includes swirl nozzle technique¹²⁻¹⁵, step nozzle technique¹⁶⁻²⁰, multiports nozzle²¹, and oval offset bore throttle plate^{22,23}. The fluid flow in the continuous casting mold can be investigated by mathematical modeling²⁴⁻²⁹, physical modeling³⁰⁻³⁹, or industrial trials⁴⁰⁻⁴². Mathematical modeling is an effective, inexpensive tool to get information that cannot be directly measured in the steel.

In the current study, industrial measurement of inclusions and total oxygen in a Low Carbon Al-killed steel are measured. The steady flow in the SEN and the strand of the continuous caster is simulated with a 3-D finite-difference computational model using the standard k- ϵ turbulence model in Fluent⁴³. Inclusion trajectories are calculated by integrating each local velocity, considering its drag and buoyancy forces. A "random walk" model is used to incorporate the effect of turbulent fluctuations on the particle motion.

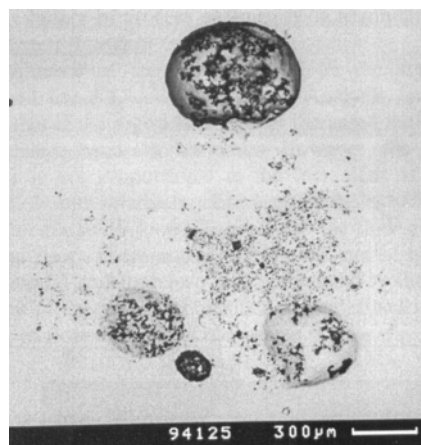


Figure 1. Inclusions attached on bubbles in a CC slab¹⁰

MATHEMATICAL MODEL OF FLUID FLOW AND INCLUSION MOTION

Mathematical Models- Modulation The continuity equation and Navier-Stokes equations for the steady fluid flow of incompressible Newtonian fluids are

$$\frac{\partial}{\partial x_i}(\rho u_i) = 0 \quad (1)$$

$$\frac{\partial}{\partial x_i}(\rho u_i u_j) = -\frac{\partial P}{\partial x_i} + (\mu_o + \mu_t) \frac{\partial}{\partial x_j} \left(\frac{\partial u_i}{\partial x_j} + \frac{\partial u_j}{\partial x_i} \right) + \rho g_i + F_j \quad (2)$$

where ρ , liquid density (kg/m³); u_i , velocity component in x_i direction (m/s); P , pressure field (N/m²); μ_o , laminar viscosity (kg/m-s); μ_t , turbulence viscosity (kg/m-s); g_j , magnitude of gravity in j direction (m/s²); F_j , other body forces (eg. from electromagnetic forces); i, j , coordinate direction indices, which when repeated in a term, implies the summation of all three possible terms. With the k - ε Model⁴⁴, the turbulent viscosity is given by

$$\mu_t = \rho C_\mu \frac{k^2}{\varepsilon} \quad (3)$$

where C_μ , empirical constant = 0.09; k , turbulent kinetic energy field, m²/s²; ε , turbulent dissipation field, m²/s³. The two additional partial differential equations for the transport of turbulent kinetic energy and its dissipation rate are given by:

$$\rho u_j \frac{\partial k}{\partial x_j} = \frac{\partial}{\partial x_j} \left(\frac{\mu_t}{\sigma_k} \frac{\partial k}{\partial x_j} \right) + \mu_t \frac{\partial \nu_j}{\partial x_i} \left(\frac{\partial u_i}{\partial x_j} + \frac{\partial u_j}{\partial x_i} \right) - \rho \varepsilon \quad (4)$$

$$\rho \nu_j \frac{\partial \varepsilon}{\partial x_j} = \frac{\partial}{\partial x_j} \left(\frac{\mu_t}{\sigma_\varepsilon} \frac{\partial \varepsilon}{\partial x_j} \right) + C_1 \mu_t \frac{\varepsilon}{K} \frac{\partial u_i}{\partial x_i} \left(\frac{\partial u_i}{\partial x_j} + \frac{\partial u_j}{\partial x_i} \right) - C_2 \frac{\varepsilon}{K} \rho \varepsilon \quad (5)$$

where $\partial/\partial x_i$, differentiation with respect to coordinate direction x, y , or z (m); $\sigma_k, \sigma_\varepsilon$, empirical constants (1.0, 1.3); C_1, C_2 , empirical constants (1.44, 1.92). The k - ε Model needs special “wall functions” as boundary conditions, in order to achieve reasonable accuracy on a coarse grid.⁴³

The trajectory of each particle can then be calculated incrementally by integrating its local velocity. The local velocity of inclusions is represented by Eq.(6) considering the force balance between drag force and the gravitational force.

$$\frac{du_{pi}}{dt} = \frac{3}{4} \frac{1}{d_p} \frac{\rho}{\rho_p} C_D (u_{pi} - u_i)^2 - \frac{(\rho - \rho_p)}{\rho_p} g_i \quad (6)$$

where ρ_p and ρ , the particle and liquid densities, kg/m³; $u_{p,i}$, the particle velocity, m/s; C_D , the drag coefficient as a function of particle Reynolds number, given as below

$$C_D = \frac{24}{Re_p} (1 + 0.186 Re_p^{0.653}) \quad (7)$$

A “random walk” model is used to incorporate the effect of turbulent fluctuations on the particle motion. In this model, particle velocity fluctuations are based on a Gaussian-distributed random number, chosen according to the local turbulent kinetic energy. The random number is changed, thus producing a new instantaneous velocity fluctuation, at a frequency equal to the characteristic

lifetime of the eddy. The instantaneous fluid velocity can be represented by

$$u = \bar{u} + u' \quad (8)$$

$$u' = \xi \sqrt{u'^2} = \xi \sqrt{2k/3} \quad (9)$$

where u : the instantaneous fluid velocity, m/s; \bar{u} : the mean fluid phase velocity, m/s; u' : random velocity fluctuation, m/s; ξ : the random number.

As boundary conditions for the particle motion, particles escape at the top surface and the open bottom, are reflected at symmetry plane, and are entrapped when they touch wide faces and narrow faces which represent the dendritic solidification front. This trapping boundary condition is valid for particles smaller than the primary dendrite arm spacing and has been employed by several researchers⁴⁵⁻⁴⁷. However, particles touching the solidifying front are not always engulfed. The entrapment phenomenon is very complex and is receiving well-deserved attention in recent work.⁴⁸⁻⁵⁰ The parameters of the SEN and the caster are shown in **Table 1**.

SEN	
Parameters	Value
SEN bore diameter, length (mm)	80, 1292
SEN submergence depth (mm)	300
Port width × port height (mm×mm)	65 × 80
Port thickness (mm)	30
Bottom well depth (mm)	10
Mold	
Parameters	Value
Nozzle port angle	Down 15°, up 15°, zero
Submergence depth (m)	0.05, 0.10, 0.15, 0.20, 0.25, 0.3
Domain height/width/thickness (m)	2.55/1.3/0.25
Casting speed (m/min)	2.0, 1.6, 1.2, 0.8
Particle diameter (μm)	300, 200, 50, spherical
Fluid density (kg/m ³)	7020
Fluid kinetic viscosity (m ² /s)	0.954×10 ⁻⁶
Particle density (kg/m ³)	3500
Argon bubble density (kg/m ³)	1.6228
Argon bubble size (mm)	1-10
Inclusion motion model	Random walk, 200 tries, 10000 inclusions

Table 1. Parameters of the SEN and continuous caster

INTERACTION BETWEEN BUBBLE AND INCLUSION IN THE MOLTEN STEEL

The attachment process of an inclusion to a gas bubble in the molten steel proceeds through the following steps: The inclusion approaches the gas bubble. If the liquid thin film between the particle and the bubble decreases to less than a critical thickness during the contact time between the bubble and the inclusion, i.e., the sliding time of the inclusion on the surface of the bubble, it will suddenly rupture causing the inclusion to attach permanently to the surface of the bubble. Otherwise, the inclusion will move away from the bubble. The critical film thickness and film rupture time are calculated elsewhere.¹⁾

In order to calculate the interaction time and the attachment probability of inclusions to the bubble surface,

a computational simulation of turbulent flow around an individual bubble and a simulation of inclusion transport through the flow field are required. First, the steady turbulent fluid flow of the molten steel around an argon bubble is calculated, assuming axi-symmetry. Possible deformation of the bubble shape by the flow and inclusion motion is ignored. The far-field velocity condition is set to be of the bubble terminal velocity, assuming a suitable turbulent energy and dissipation rate, and a far field pressure outlet. Then the inclusion trajectories around the bubble are calculated. Several thousand inclusions are uniformly injected into the domain in the column with diameter far larger than d_B+d_p from the place of the 15-20 times of the bubble diameter far from the bubble center. As boundary conditions, inclusions reflect if they touch the surface of the bubble. If the normal distance of the inclusion center to the surface of the bubble is first less than the inclusion radius, the collision between the inclusion and the bubble takes place. And if this distance keeps less than the inclusion radius for some time, then it is the sliding time. Inclusions will be attached to the surface of the bubble according to the criterion discussed before. Then the attached probability, as shown in **Figure 2**, can be expressed by

$$P = \frac{\dot{a}_i P_{A_i}}{A_{B+p}} = \frac{\dot{a}_i \frac{\dot{N}_{o,i}}{\dot{N}_{T,i}} (p(R_i + DR)^2 - pR_i^2)}{p(d_B + d_p)^2} \quad (10)$$

where N_o is the number of inclusions attaching to the bubble by satisfying that their contact time is larger than the film rupture time. A_{B+p} is the section area of the column with diameter of d_B+d_p . $N_{T,i}$ is the total number of inclusions injected through the area A_i , and i is the sequence number of the annular position at which the inclusions are injected.

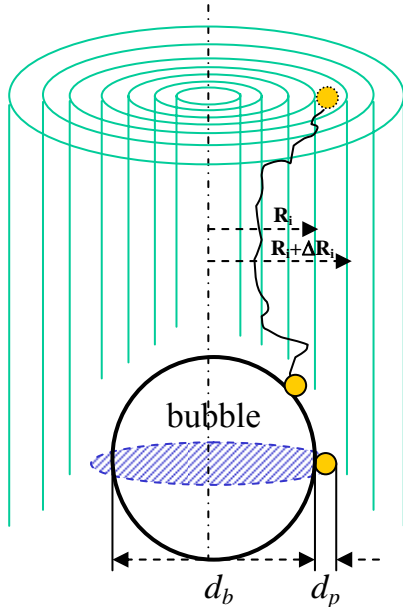


Figure 2. Schematic of the attachment probability of inclusions to the bubble surface under stochastic turbulent effect

A removal model of inclusions by bubble flotation is developed for the molten steel-alumina inclusions-argon bubbles system. The following assumptions are used:

- Bubbles all have the same size;
- Inclusions have a size distribution and are uniformly distributed in the molten steel, and they are too small to affect bubble motion or the flow pattern;
- The bubble size and the gas flow rate are chosen independently;
- Once stable attachment occurs between a bubble and an inclusion, there is no detachment and the inclusion is considered to be removed from the molten steel, owing to the high removal fraction of most bubbles.

Assuming that all inclusions are Al_2O_3 , the total oxygen (in ppm) removed by bubble flotation can be expressed by

$$\Delta O = 1.16 \times 10^5 \cdot \frac{1}{V_C S} \cdot \frac{d_B^2 L_B}{t_B} \cdot \frac{\rho_p}{\rho_M} \sum_{j=1}^{n_B} \left[\sum_i (n_{p,i}|_j \cdot P_{A_i} \cdot d_{p,i}^3) \right] \quad (11)$$

$$n_{p,i}|_j = n_{p,i}|_{j-1} \times \frac{(100 - P_{A_i})}{100} \times \frac{\left(\frac{\pi d_B^2}{4} \right) L_B}{V_C S \cdot t_B} \quad (12)$$

$$n_B = \frac{3}{273\pi} Q_G T_M \frac{t_B}{d_B^3} \quad (13)$$

where d_B is the bubble diameter (m), L_B is the path length of the bubble (m), t_B is the bubble residence time (s), P_A is the attachment probability of the inclusion to the bubble (%), and n_p is the number density of that inclusion size (number/m³ steel), V_C is casting speed (m/min), S is the area of the slab section ($=0.25 \times 1.3m^2$), ρ_p and ρ_M are densities of inclusions and the molten steel. n_B is the number of bubbles in the domain during time t_B , Q_G is the gas flow (Nl/min), T_M is the steel temperature (1823K).

$n_{p,i}|_j$ is the number density of inclusion with diameter $d_{p,i}$ when bubble j is injected, used to update the inclusion number density distribution after the calculation of each individual bubble in order to account for the significant change in inclusion concentration caused by the simultaneous inclusion removal of many bubbles.

FLUID FLOW AND INCLUSION MOTION IN SEN REGION

The simulation domain is shown in **Figure 3**. In the current simulation, the SEN and the mold is combined together. The effect of annular steps on the fluid flow and inclusion motion in the SEN and caster strand are investigated. Two annular steps in a SEN (Step SEN) is calculated. Due to the sharp decreasing of the bore diameter at the steps, the fluid flow is accelerated at these locations in the Step SEN. This acceleration helps to diminish the non-uniform velocities generated by the slide gate. Near the slide gate, inclusions may have slight recirculation, as shown in **Figure 3**.

Without steps, the uneven flow passing the slide gate finally generates a swirl at the bottom of the nozzle, therefore the molten steel enters mold with swirl, as shown in **Figure 3** and **Figure 4**. This swirl at the bottom and outports are diminished in the Step SEN. Jet characteristics for nozzles with outports angle of 15°, down, 0° horizontal, 15° up, and Steps are compared in **Table 2**. The 15° down nozzle with two steps has the smallest turbulent energy and dissipation rate, which means the jet entering the mold has the weakest turbulence. The jet angle is only 18° for the Step SEN (Down 15°), compared with 29° without steps (Down15°),

and 18° for Zero degree angle nozzle without Steps. The large jet angle corresponds to a large impingement depth, therefore worsens the inclusion removal to the top surface. One problem of the Step SEN is its large back flow zone fraction, 30%, compared with all three conventional nozzles in **Table 2**. Larger back-flow zone will bring more inclusions back to the outport region of SEN, possibly inducing clogging there. The step nozzle may have more inclusion removal to the top surface of the mold perhaps by eliminating swirls at SEN outports and in the mold, and by decreasing the impingement depth of the jet in the mold. For the down 15° angle nozzle, only 17% of the 50μm inclusions are removed to the top surface, but this number increases to 31% with two annular steps, as shown in **figure 5**. Zero angle nozzle and up 15° nozzle have a slight larger inclusion removal fraction to the top, ~20-22%. Because the inclusion removal rates are so small for all nozzles, it is more important to choose nozzle designs that produce optimal conditions at the meniscus to avoid slag entrainment, level fluctuations, and other problems.



Figure 3. Simulation domain (left), swirl pathline at the outport of SEN (middle), and inclusion trajectories near the slide gate

SEN Outport angle	Down15	Down 15	Zero	Up 15
With steps or not	No	2 Steps	No	No
Weight mean x velocity (m/s)	0.80	0.96	0.87	0.86
Weight average y velocity (m/s)	-0.0351	0.012	0.0018	-0.007
Weight average z velocity (m/s)	0.45	0.32	0.14	0.28
Weight average turbulent energy (m ² /s ²)	0.27	0.20	0.32	0.31
Weight average turbulent energy dissipation rate (m ² /s ³)	6.41	5.27	10.47	8.88
Vertical jet angle (°)	29.29	18.23	9.10	17.76
Horizontal jet angle (°)	-2.52	0.72	0.12	-0.47
Jet speed (m/s)	0.92	1.01	0.89	0.90
Back-flow zone fraction (%)	15.31	29.38	26.15	20.73
Swirl or not at Outports	With	No	With	With

Table 2 Jet characteristics of SEN with different outports angle and steps in nozzle ($V_c=1.2\text{m/min}$, Submergence depth=300mm)

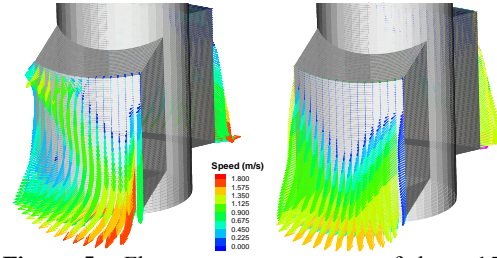


Figure 5. Flow pattern at outports of down 15° angle without steps (left) and with steps (right) ($V_c=1.2\text{m/min}$, Submergence depth=300mm)

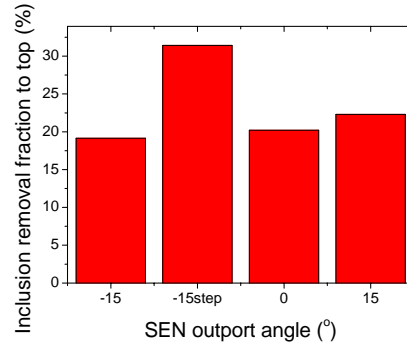


Figure 5. 50μm inclusion removal to the top of the mold with different port angle SEN ($V_c=1.2\text{m/min}$, Submergence depth=300mm)

FLUID FLOW AND INCLUSION MOTION IN MOLD REGION

The velocity vector distribution on the center face of the half strand is shown in **Figure 6**, indicating a double roll flow pattern. The upper loop reaches the meniscus of the narrow face, and the second loop takes steel downwards into the liquid core and eventually flows back towards the meniscus in the strand center. The calculated weighted average turbulent energy and its dissipation rate in the CC strand are $1.65 \times 10^{-3} \text{ m}^2/\text{s}^2$ and $4.22 \times 10^{-3} \text{ m}^2/\text{s}^3$ respectively.

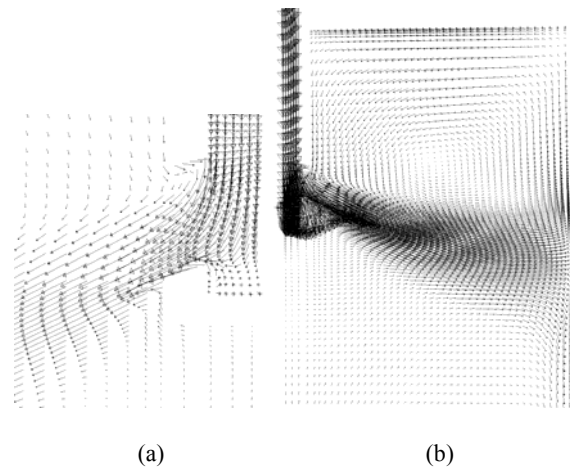


Figure 6. Fluid flow in continuous casting strands with half depth, a: velocity near the SEN outport; b: velocity on the center face (300mm submergence depth, 1.2 m/min casting speed, and no gas injection)

The calculated typical random trajectories of bubbles and inclusions are show in **Figure 7**. Smaller particles penetrate and circulate more deeply than the larger ones.

Bubbles larger than 1mm mainly move in the upper roll. 0.2mm bubbles can move with paths as long as 6.65m and 71.5s before they escape from the top or become entrapped through the bottom, while 0.5mm bubbles move 3.34m and 21.62s, 1mm bubbles move 1.67m and 9.2s, and 5mm bubbles move 0.59m 0.59s.

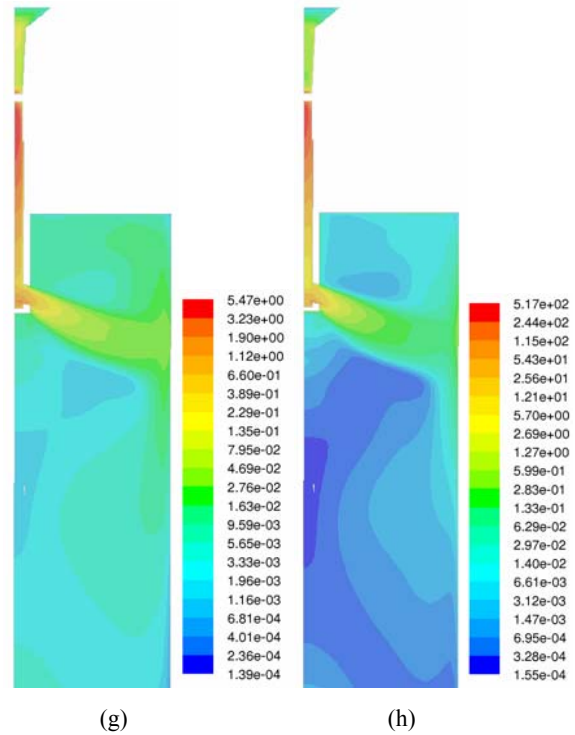
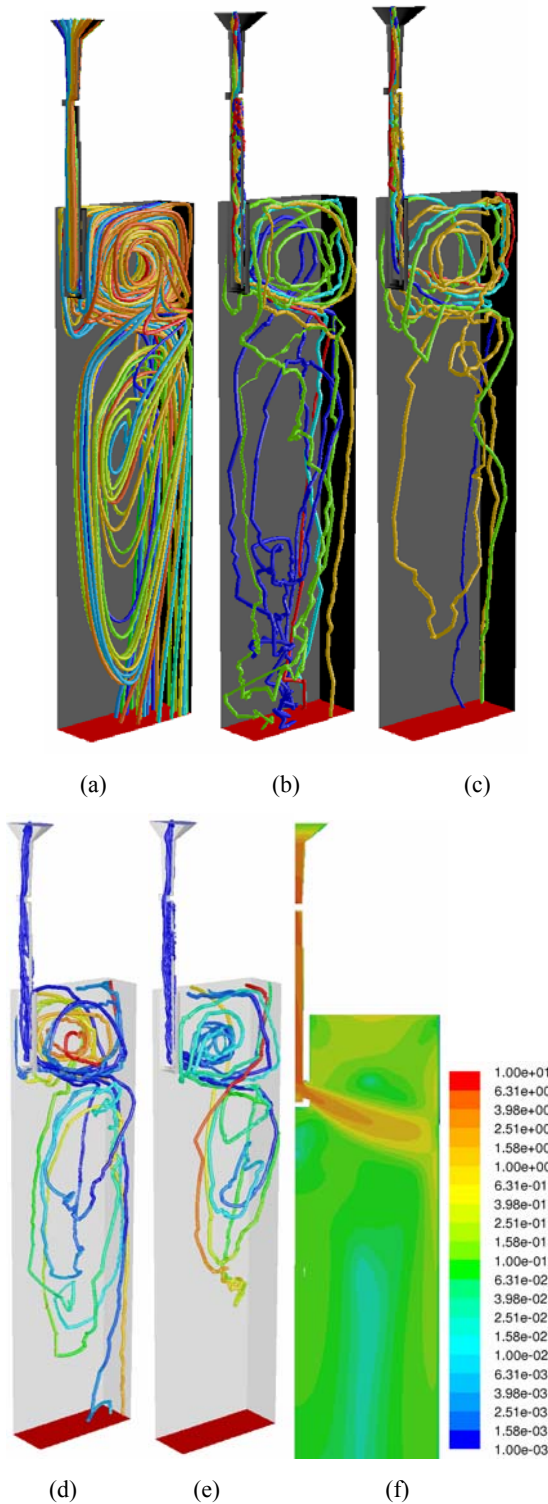


Figure 7. Fluid flow in continuous casting strands (300mm submergence depth, 1.2 m/min casting speed, and no gas injection) (a: pathline, b: trajectories of 50µm inclusions, c: trajectories of 300µm inclusions, d: trajectories of 0.2mm bubbles, e: 1mm bubbles, f: fluid flow speed (m/s), g: turbulent energy (m²/s²), h: turbulent energy dissipation rate (m²/s³)

Computed locations of inclusions attached to the SEN walls and entrapped at the wide faces of the slab are shown in **Figure 8**. The calculation suggests that around 4% inclusions leaving the tundish stick to the SEN walls, i.e., removal by clogging. Fig.8 suggests roughly uniform buildup on the nozzle walls, with increased tendency towards buildup on the SEN bottom due to impact from the flowing jet. This is consistent with observations of nozzle clogging where local reoxidation or chemical interaction were not the cause.

The majority of inclusions leaving the tundish (more than 50%) are captured within 30mm of the surface, which represents the top 2.55m of the caster. Fig. 8 also shows that inclusion accumulation peaks are at 12-14mm below the surface of the slab. A disproportionately large fraction of these (15-16%) are captured in the narrow face, despite its smaller surface area, owing to the jet impingement against its inner solidification front. 25-28% inclusions exiting the domain are entrapped somewhere deeper in the interior than 30mm shell thickness. A larger fraction of inclusions bigger than 50 µm are removed. For example, 10% 225 µm inclusions leaving the tundish are removed to the top of the mold by fluid flow transport. The calculated inclusion removal from tundish to slab by fluid flow transport, summing up to SEN walls and the top surface of the mold, is 10-14%. Large inclusions (300µm) more tend to remove to the top, and small inclusions (50µm) recirculate more and most of them are flow out from the bottom.

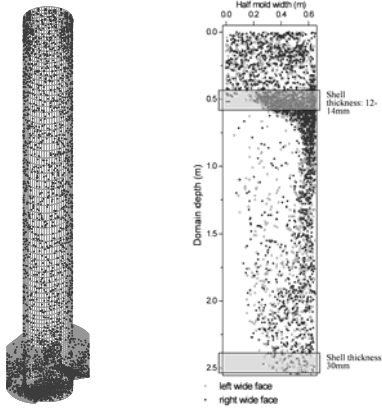
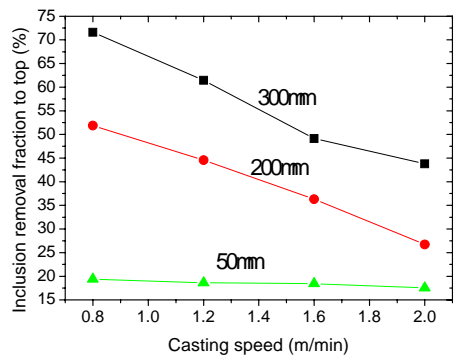
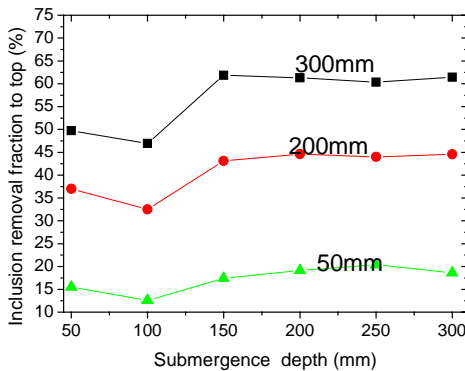


Figure 8. Inclusion locations sticking to SEN walls (left) and to wide faces of the slab (right)

Inclusion removal fraction to the top as function of casting speed, inclusion size and submergence depth is shown in **Figure 9**. The removal fraction of $<50\mu\text{m}$ inclusions is independent of casting speed. Large inclusions are removed more with decreasing casting speed, and large inclusions are more easily removed. It should be noticed that inclusions as large as $200\mu\text{m}$ can only removed less than 75% due to the strong turbulence in the mold region and small residence time of the molten steel in the mold region. The calculated inclusion removal fraction as function of submergence depth is a little surprising because it indicates that larger submergence depth removes a little more inclusions. This needs further investigation to explain.



(a) Submergence depth = 150mm



(b) Casting speed = 1.2m/min

Figure 9. Inclusion removal fraction as function of casting speed, inclusion size, and submergence depth

INTERACTION BETWEEN INCLUSION AND BUBBLE IN MOLTEN STEEL

Figure 10 shows the fluid flow pattern and trajectories of $100\mu\text{m}$ inclusions around a 5mm bubble in molten steel. Inclusions tend to touch the bubble after the top point. Stochastic fluctuation of the turbulence makes the inclusions very dispersed, so attachment may occur at a range of positions. Calculation indicates that the average turbulent energy in the domain has little effect on the final turbulent energy distribution around the bubble.

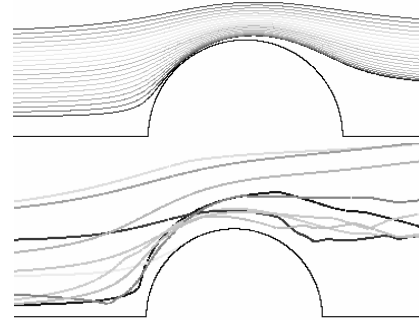


Figure 10. Trajectories of $100\mu\text{m}$ inclusions around a 5mm bubble in the molten steel (up: non-stochastic model, lower: stochastic model)

The attachment probability of inclusions ($d_p=5, 10, 20, 35, 50, 70, 100\mu\text{m}$) to bubbles (1, 2, 4, 6, 10mm) are calculated by the trajectory calculation of inclusions, which indicates that smaller bubbles and larger inclusions have larger attachment probabilities. 1mm bubbles can have inclusion attachment probability as high as 30%, while the inclusion attachment probability to $>5\text{mm}$ bubbles is less than 1%. To enable the computation of attachment rates for a continuous size distribution of inclusions and bubbles, regression is performed on these calculated attachment probability of inclusions ($d_p=5, 10, 20, 35, 50, 70, 100\mu\text{m}$) to bubbles (1, 2, 4, 6, 10mm), obtaining the following equation:

$$P_A = Ad_p^B \quad (14)$$

where A and B depend on inclusion size. In Eq.(11), P_A is calculated by this equation.

The corresponding inclusion removal fractions by bubble flotation in the continuous casting strand are shown in **Figure 11**. Smaller bubbles appear to cause more inclusion removal with the same gas flow rate. Specifically, 1mm bubbles remove almost all of the inclusions larger than $30\mu\text{m}$. However, it is unlikely that all of these small bubbles could escape from the top surface. Those that are entrapped in the solidifying shell would generate serious defects in the steel product. Increasing bubble size above $\sim 7\text{mm}$ produces no change in removal rate, likely due to the change in bubble shape offsetting the smaller number of bubbles. Thus, there should be an optimum bubble size, which gives not only high inclusion removal efficiencies, but also low entrapment rates. The present results suggest an optimal range of perhaps 2-4mm. As shown in Fig.11, increasing gas flow rate causes more inclusion removal by bubble flotation. The effect of turbulent Stochastic motion slightly increases the inclusion removal by bubble flotation. For the current CC conditions, including a gas flow rate of 15 Nl/min , the bubble size is likely to be around 5mm, assuming that there are a large number of

active sites on the porous refractory that cause a gas flow rate of <0.5 ml/pore.⁵¹⁾ As shown in Fig. 11, about 10% total oxygen is removed by bubble flotation. This corresponds to a 3ppm decrease in total oxygen. It has been predicted that 6-10% inclusions are removed to the top surface due to flow transport in the CC mold region. Thus, the total predicted inclusion removal by flow transport and by bubble flotation is around 16-20%.

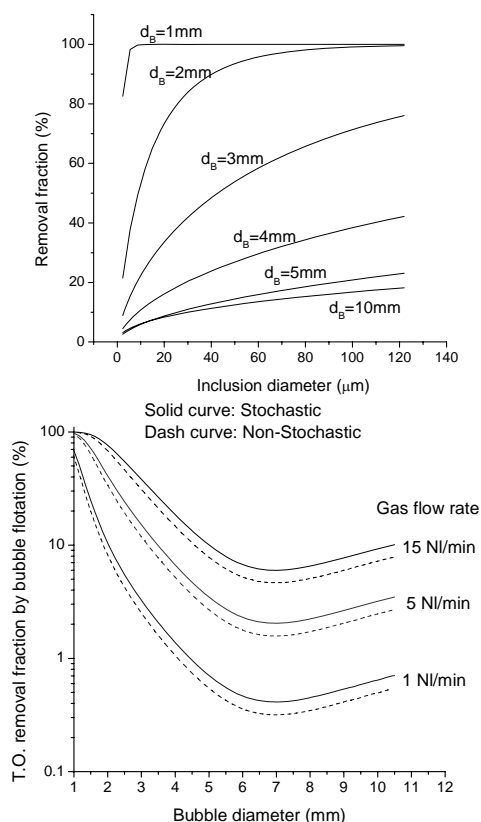


Figure 11. Calculated inclusion removal by bubble flotation (15 NI/min gas in left figure)

INDUSTRIAL TRIALS OF INCLUSION MEASUREMENTS

The total oxygen in a Low Carbon Al-killed steel are measured, as shown in **Table 3**. Steady casting period has a better cleanliness than unsteady casting period (cast start, cast end and ladle change). And outer surface of the slab has large total oxygen than its inside. Inclusions extracted by Slimes test at the casting condition of 1.2m/min speed and 150mm SEN submergence depth were suspended in water and their size distributions measured with a Coulter counter to get a 3-dimensional inclusion size distribution. This obtained the 3-dimensional size distribution up to 62 μ m. The curves were extrapolated to around 120 μ m as given in **Figure 12** by matching to the measured amount of extracted inclusions larger than 50 μ m. The inclusions mass fraction is 66.8ppm in the tundish, 57.7ppm in the 20mm thickness nearest the slab surface, and averaging 51.9ppm in the slab. This suggests that inclusions in the interior of the slab (i.e., except outer 20mm thickness of the slab) is 50.6ppm. The fraction of inclusions removed from tundish to slab is around 22%.

The numerical prediction and the measurement agree remarkably well, considering that 4% inclusions are entrapped to the SEN walls to cause clogging.

	First cast sequence			
	1	2	3	4
Inner surface	0.004	0.0017	0.0015	0.0018
1/4 thickness	0.0046	0.0014	0.0026	0.0029
Center	0.0034	0.0015	0.0018	0.0023
3/4 thickness	0.0031	0.0013	0.0024	0.0023
Outer surface	0.004	0.0021	0.0014	0.0018
mean	0.0038	0.0016	0.0019	0.0022
	Second cast sequence			
	1	2	3	4
Inner surface	0.0033	0.002	0.0018	0.0016
1/4 thickness	0.0028	0.0028	0.0021	0.0019
Center	0.0033	0.0026	0.002	0.0021
3/4 thickness	0.0029	0.002	0.0016	0.0018
Outer surface	0.0045	0.0022	0.0016	0.002
mean	0.0034	0.0023	0.0018	0.0019

1: First slab of first heat; 2: Second slab of second heat; 3: Slab between 2 and 3 heats; 4: End of third heat

Table 3. Slab total oxygen measurement (%)

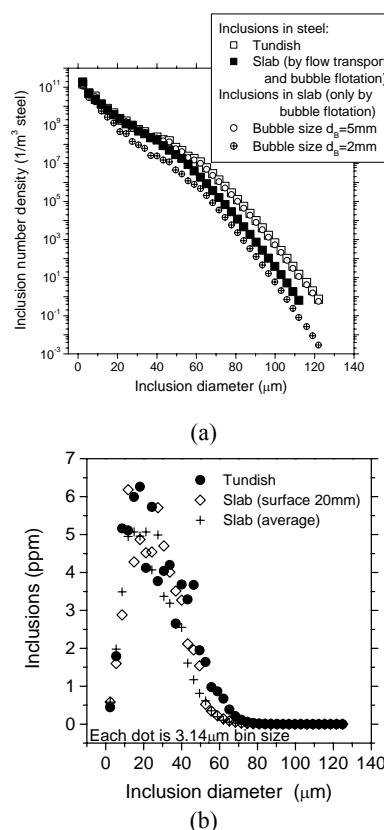


Figure 12. Inclusion size distribution evolution by Coulter Counter measurement of the Slime extracted inclusions

The measured inclusion distribution compared with the prediction is shown in **Figure 12b**. The initial size distribution of inclusions in the simulation is the size distribution in the tundish. The predicted is the size distribution of inclusions after removed only by bubble flotation. If considering the inclusion removal by flow transport, the matching between the calculation and the measurement will be much better.

CONCLUSIONS

- 1) This work presents a fundamental model of inclusion removal by fluid flow transport and by bubble flotation in the molten steel of a continuous casting strand.
- 2) Smaller bubbles and larger inclusions have larger attachment probabilities. Bubbles smaller than 1mm diameter have inclusion attachment probabilities as high as 30%, while the inclusion attachment probability for bubbles larger than 5mm is less than 1%. The stochastic effect of turbulence (modeled by the random walk method) slightly increases the attachment rate.
- 3) In the CC strand, smaller bubbles penetrate and circulate more deeply than larger ones. Bubbles larger than 1mm mainly move in the upper roll. 0.2mm bubbles can move as far as 6.65m and take 71.5s before they either escape from the top or are entrapped through the bottom, while 0.5mm bubbles move 3.34m and take 21.62s, 1mm bubbles move 1.67m and take 9.2s, and 5mm bubbles move 0.59m and take 0.59s.
- 4) In the CC mold, if bubbles are ~ 5mm in diameter, ~10% of the inclusions are predicted to be removed by bubble flotation, corresponding to around 3ppm decrease in total oxygen. Combined with ~ 8% inclusion removal by flow transport and 4% by entrapment to SEN walls as clogging, the total roughly agrees well with the measured inclusion removal rate by the CC mold of ~22%.
- 5) Smaller bubbles are more efficient at inclusion removal by bubble flotation, so long as they are not entrapped in the solidifying shell. Larger gas flow rate favors inclusion removal by bubble flotation. The optimum bubble size should be 2-4mm.

REFERENCES

- 1) L. Zhang and S. Taniguchi: *International Materials Reviews*, (2000), 45(2), 59.
- 2) A. G. Szekely: *Metal. Trans. B*, (1976), 7B(3), 259.
- 3) K. Okumura, M. Kitazawa, N. Hakamada, M. Hirasawa, M. Sano and K. Mori: *ISIJ International*, (1995), 35(7), 832.
- 4) Y. Miki, B. G. Thomas, A. Denisov and Y. Shimada: *Iron and Steelmaker*, (1997), 24(8), 31.
- 5) W. Pan, K. Uemura and S. Koyama: *Tetsu-to-Hagane*, (1992), 78(8), 87.
- 6) L. Zhang and S. Taniguchi: *Ironmaking & Steelmaking*, (2002), Vol.29(5), 326.
- 7) R. Gass, H. Knoepke, J. Moscoe, R. Shah, J. Beck, J. Dzierzawski and P. E. Ponikvar, in *ISSTech2003 Conference Proceedings*, eds., ISS, Warrandale, PA, (2003), 3-18.
- 8) P. Rocabois, J.-N. Pontoire, V. Delville and I. Marolleau, in *ISSTech2003 Conference Proceedings*, eds., ISS, Warrandale, PA, (2003), 995-1006.
- 9) L. Zhang, B. G. Thomas and B. Rietow: *University of Illinois at Urbana-Champaign*, Report No. CCC200406, (2004).
- 10) Y. Miki: *Study on the Inclusion Removal and Bubble Behavior in the Molten Steel*, ed., eds., Kawasaki Steel, (2001).
- 11) J. Herbertson, Q. L. He, P. J. Flint and R. B. Mahapatra, in *Steelmaking Conf. Proceedings*, 74, eds., ISS, Warrendale, PA, (1991), 171-185.
- 12) S. Yokoya, R. Westoff, Y. Asako, S. Hara and J. Szekely: *ISIJ Int.*, (1994), 34(11), 889.
- 13) S. Yokoya, Y. Asako, S. Hara and J. Szekely: *ISIJ Int.*, (1994), 34(11), 883.
- 14) S. Yokoya, S. Takagi, M. Iguchi, Y. Asako, R. Bestoff and S. Hara: *ISIJ Int.*, (1998), 38(8), 827.
- 15) S. Yokoya, S. Takagi, H. Souma, M. Iguchi, Y. Asako and S. Hara: *ISIJ Int.*, (1998), 38(10), 1086.
- 16) O. Nomura: *Seramikkusu (Ceramics Japan: Bulletin of the Ceramic Spcoety of Japan)*, (2000), 35(8), 617.
- 17) S. Yokoya, S. Haseo, S. Takagi, Y. Asako, S. J and S. Hara, in *Steelmaking Conference Proceedings*, 79, eds., ISS, Warrendale, PA, Pittsburgh, PA, (1996), 217-224.
- 18) N. Tsukamoto, Y. Kurashina and K. Yanagawa: *Taikabutsu*, (1994), 46(4), 215.
- 19) N. Tsukamoto, K. Ichikawa, E. Iida, A. Morita and J. Inoue, in *74th Steelmaking Conference Proceedings*, 74, eds., ISS, Warrendale, PA, (1991), 803-808.
- 20) L. Zhang and B. G. Thomas, in *XXIV Steelmaking National Symposium Mexico*, eds., Morelia, Mich, Mexico, (2003),
- 21) K. Morward, J. Watzinger, M. Stiffinger, H. Resch and G. Shan, in *ISSTech2003*, eds., ISS, Warrandale, PA, (2003), 1135-1155.
- 22) M. R. Ozgu, W. E. Sattler, C. A. Farlow and L. J. Lawrence, in *ISSTech2003, Electric Furnace, Steelmaking*, eds., ISS, Warrandale, PA, (2003), 31-40.
- 23) P. D. King, L. J. Heaslip, D. Xu, J. D. Dorricott and Q. K. Robinson, in *ISSTech2003 Conference Proceedings, Electric Furnace and Steelmaking*, eds., ISS, Warrandale, PA, (2003), 265-282.
- 24) J. Szekely and V. Stanek: *Metall. Trans.*, (1970), 1(1), 119.
- 25) M. Yao, M. Ichimiya, M. Tamiya, K. Suzuki, K. Sugiyama and R. Mesaki: *Transactions of the Iron and Steel Institute of Japan*, (1984), 24(2), s211.
- 26) B. G. Thomas, L. J. Mika and F. M. Najjar: *Metall. Trans. B*, (1990), 21B(2), 387.
- 27) X. Huang and B. G. Thomas: *Metall. Trans.*, (1993), 24B(2), 379.
- 28) X. Huang and B. G. Thomas: *Metall. Trans. B*, (1996), 27B(4), 617.
- 29) B. G. Thomas, H. Bai, S. Sivaramkrishnan and S. P. Vanka: *International Symposium on Cutting Edge of Computer Simulation of Solidification and Processes*, I. Ohnaka, eds., ISIJ, (1999), 113-128.
- 30) K. I. Afanaseva and T. P. Iventsov: *Stal*, (1958), 18(7), 599.
- 31) J. Szekely and R. T. Yadaya: *Metall. Trans. B*, (1972), 3(5), 2673.
- 32) L. J. Heaslip, I. D. Sommerville, A. McLean, L. Swartz and W. G. Wilson: *Iron and Steelmaker (ISS Transactions)*, (1987), 14(8), 49.
- 33) H. Tanaka, H. Kuwatori and R. Nisihara: *Tetsu-to-Hagane*, (1992), 78(5), 761.
- 34) T. Teshima, J. Kubota, M. Suzuki, K. Ozawa, T. Masaoka and S. Miyahara: *Tetsu-to-Hagane*, (1993), 79(5), 576.
- 35) D. Gupta and A. K. Lahiri: *Metall. Mater. Trans. B*, (1996), 27B(5), 757.
- 36) L. J. Heaslip and J. Schade: *Iron and Steelmaker (ISS Transactions)*, (1999), 26(1), 33.

- 37) M. Iguchi, J. Yoshida, T. Shimzu and Y. Mizuno: *ISIJ Int.*, (2000), 40(7), 685.
- 38) P. H. Dauby, M. B. Assar and G. D. Lawson: *Rev. Met.*, (2001), 98(4), 353.
- 39) J. Yoshida, M. Iguchi and S. Yokoya: *Tetsu-to-Hagane*, (2001), 87(8), 529.
- 40) P. H. Dauby, D. F. Havel and P. A. Medve, in *73rd Steelmaking Conference Proc.*, 73, eds., ISS, Warrendale, PA, (1990), 33-39.
- 41) M. B. Assar, P. H. Dauby and G. D. Lawson, in *Steelmaking Conference Proceedings*, 83, eds., ISS, Warrendale, PA, (2000), 397-411.
- 42) P. H. Dauby and S. Kunstreich, in *ISSTech2003*, eds., ISS, Warrandale, PA, (2003), 491-503.
- 43) *FLUENT5.1: Fluent Inc.*, Lebanon, New Hampshire, Report No., (2000).
- 44) B. E. Launder and D. B. Spalding: *Computer Methods in Applied Mechanics and Engr.* (1974), 13(3), 269.
- 45) B. Grimm, P. Andrzejewski, K. Muller and K.-H. Tacke: *Steel Res.*, (1999), 70(10),
- 46) B. Grimm, P. Andrzejewski, K. Wagner and K.-H. Tacke: *Stahl und Eisen*, (1995), 115(2), 71.
- 47) M. R. Aboutalebi, M. Hasan and R. I. L. Guthrie: *Metall. Mater. Trans. B*, (1995), 26B(4), 731.
- 48) M. Yemmou, M. A. A. Azouni and P. Casses: *Journal of Crystal Growth*, (1993), 128(4), 1130.
- 49) J. K. Kim and P. K. RRRohatgi: *Metall. & Mater. Trans. B*, (1998), 29A(1), 351.
- 50) D. M. Stefanescu and A. V. Catalina: *ISIJ Int.*, (1998), 38(5), 503.
- 51) H. Bai and B. G. Thomas: *Metall. Mater. Trans. B*, (2001), 32B, 1143.